

***In situ* regeneration of copper catalysts for long-term electrochemical CO₂ reduction to multiple carbon products**

Cornelius Obasanjo,¹ Ali Shayesteh Zeraati,² Hadi Shaker Shiran,² Tu N. Nguyen,^{1,3} Sharif Md. Sadaf,⁴ Md Golam Kibria,^{2,*} Cao-Thang Dinh^{1,*}

¹Department of Chemical Engineering, Queen's University, Kingston, ON, K7L 3N6, Canada.

²Department of Chemical and Petroleum Engineering, University of Calgary, 2500 University Drive, NW Calgary, Alberta, Canada, T2N 1N4

³Helen Scientific Research and Technological Development Co., Ltd, Ho Chi Minh City 700000, Vietnam.

⁴Centre Energie, Matériaux et Télécommunications, Institut National de la Recherche Scientifique (INRS)-Université du Québec, 1650 Boulevard Lionel-Boulet, Varennes, Quebec J3X 1S2, Canada.

Emails: md.kibria@ucalgary.ca; caothang.dinh@queensu.ca

Supplementary Information.

1. Cu catalyst layer thickness measurement.

The metal film thickness of each Cu deposition was measured using a small piece of silicon wafer placed near the sample's edge during deposition. Each silicon piece was patterned with negative photoresist AZ nLOF 2020 using contact photolithography. Following metal deposition, the resist was lifted off in a bath of photoresist stripper (N-methylpyrrolidinone) at 75°C to leave a pattern of small metal rectangles on silicon. The sharp step edges produced in this approach improve the accuracy of the step height measurement by stylus profilometry, which was performed using a Bruker Dektak XT profilometer. The thickness of the metal film on the test chip was determined as the mean of step height measurements from six different profiles.

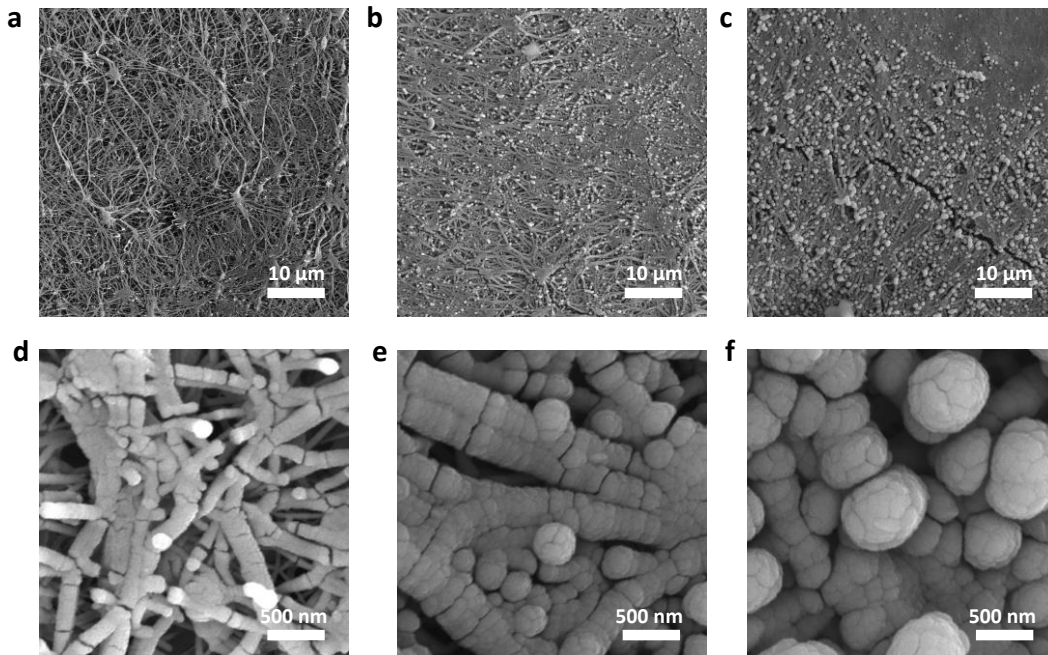


Fig. S1. Scanning electron microscopy (SEM) images of Cu/PTFE with Cu nominal thickness of 200 nm (a and d), 700 nm (b and e), and 1000 nm (c and f). Fig. S1f is the same as figure 2c in the manuscript. It is included here for the purpose of comparison.

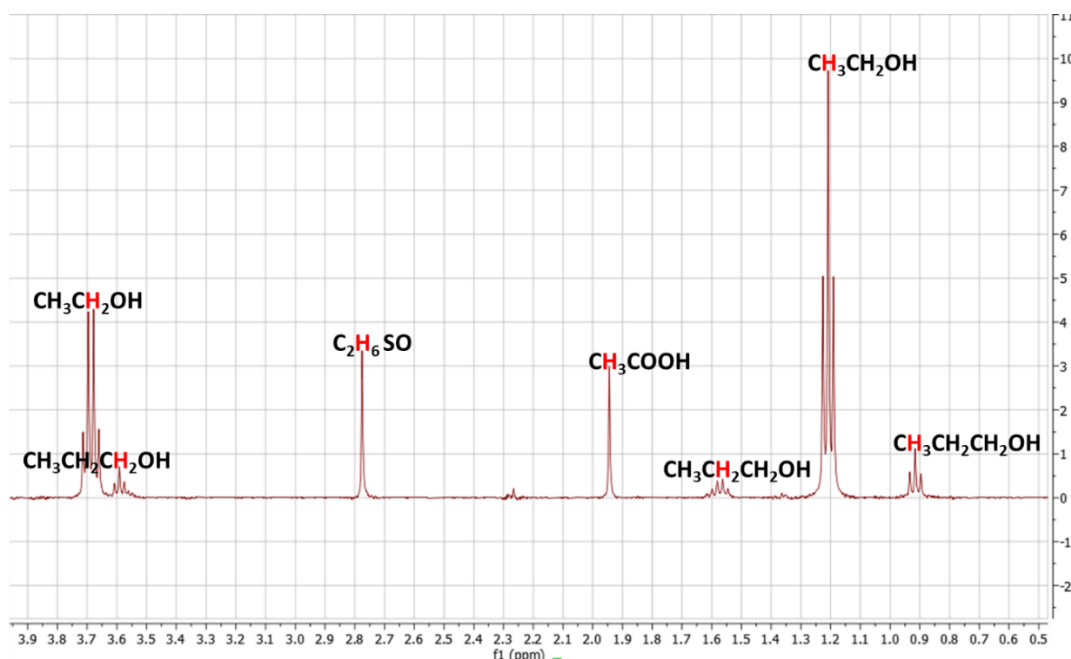


Fig. S2. ^1H NMR spectrum of a representative liquid product analysis. Data collected from the spectrum were used in the calculation of the Faradaic efficiency (FE) for the liquid product analysis.

Table S1. Cathodic potential data of electrochemical CO_2 reduction reactions for 200, 700, and 1000 nm Cu samples at different current densities. Collected potential values are represented in V (vs Ag/AgCl). The experiments were conducted using 1M KHCO_3 and 1M KOH as catholyte and anolyte respectively. A bipolar membrane was used.

Cu catalyst thickness (nm)		Cathodic potential (V vs Ag/AgCl)		
		200	700	1000
Current density (mA cm^{-2})	100	-2.80 ± 0.03	-2.55 ± 0.06	-2.46 ± 0.03
	150	-3.39 ± 0.03	-3.07 ± 0.05	-3.05 ± 0.06
	200	-3.87 ± 0.10	-3.76 ± 0.31	-3.64 ± 0.09
	250	-4.44 ± 0.13	-4.22 ± 0.13	-4.23 ± 0.14

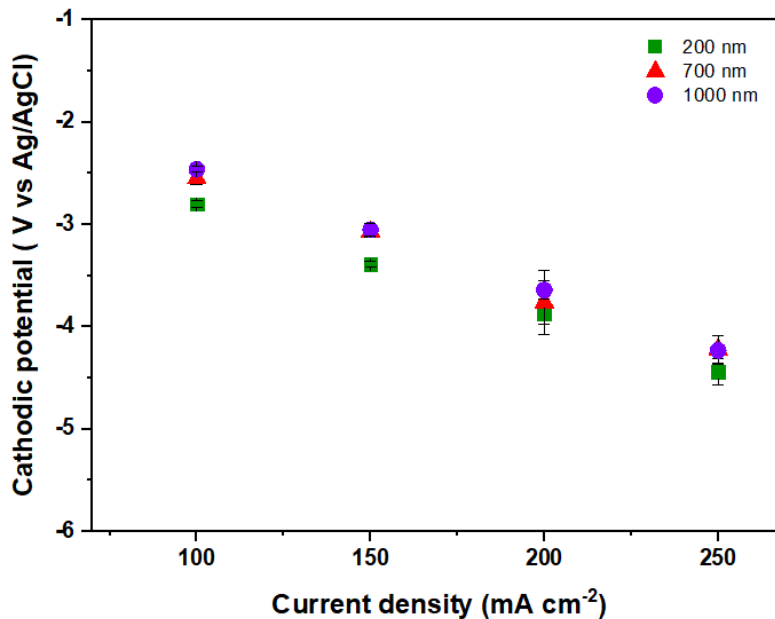


Fig. S3. Cathodic potential vs current density plot of electrochemical CO₂ reduction reactions for 200, 700 and 1000 nm Cu samples at different current densities.

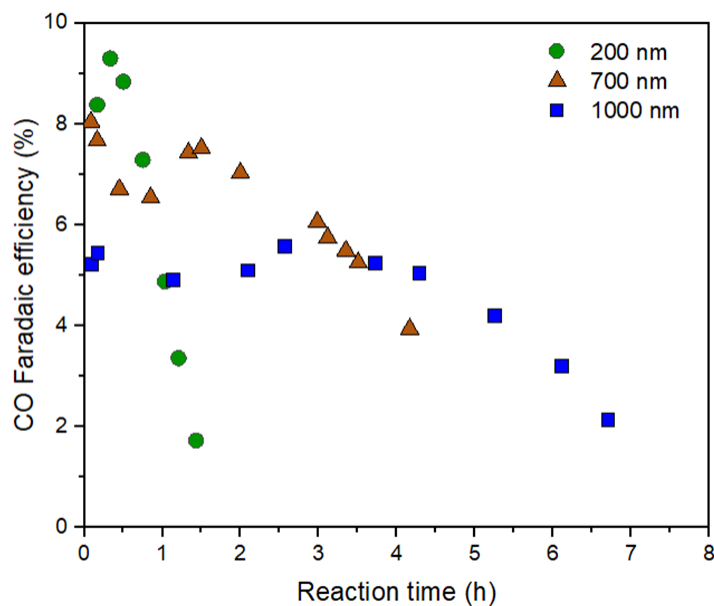


Fig. S4. Variation of CO FE over reaction time at a constant current density of 150 mA cm⁻² in 1M KHCO₃ electrolyte. Electrochemical measurements were conducted in a customized 3-electrode flow-type cell using a bipolar membrane. The choice of membrane used improves the overall cell energy efficiency and ensures that there is no reactant and product crossover to the anode compartment from the cathode side.

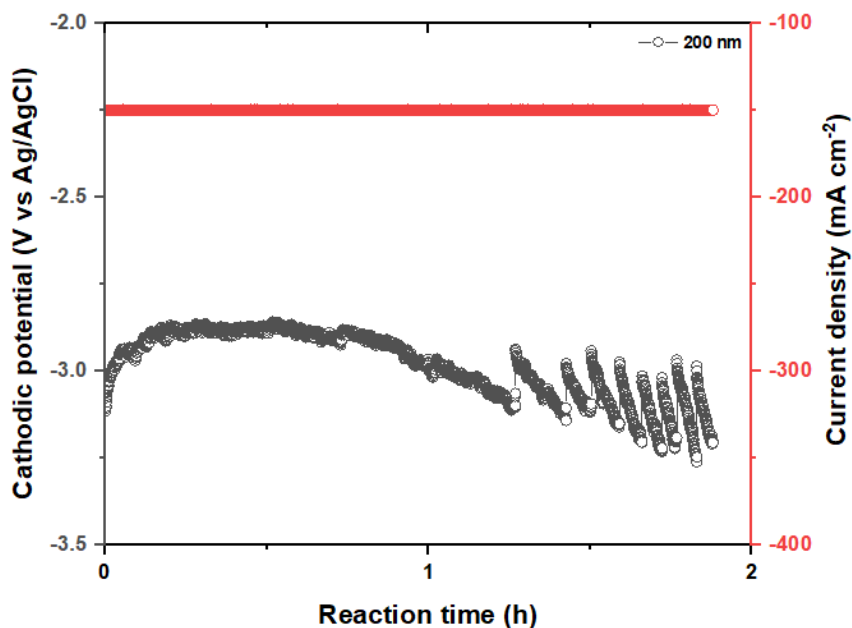


Fig. S5. Potential data of continuous electrochemical CO₂ reduction reactions at -150 mA cm⁻² on 200nm Cu sample. 1M KHCO₃ and 1M KOH electrolytes were used as catholyte and anolyte, respectively.

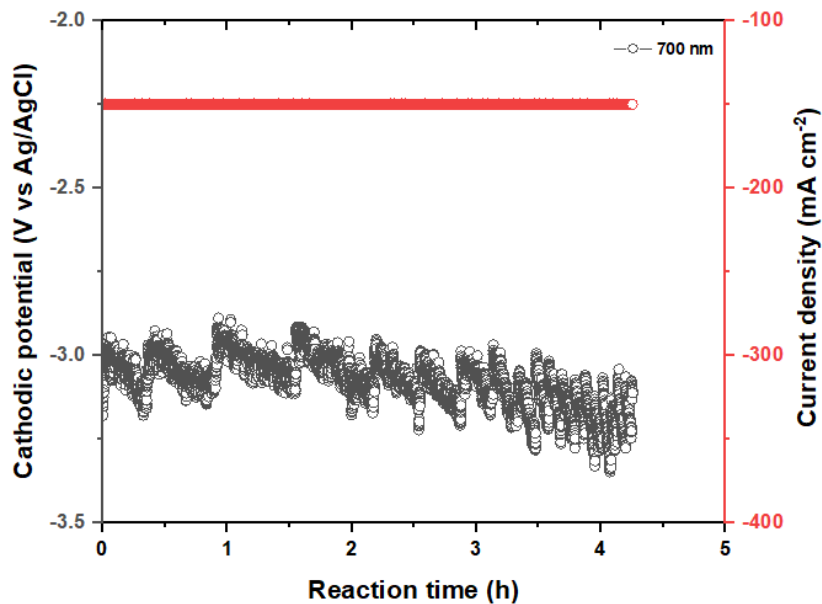


Fig. S6. Potential data of continuous electrochemical CO₂ reduction reactions at -150 mA cm⁻² on 700nm Cu sample. 1M KHCO₃ and 1M KOH electrolytes were used as catholyte and anolyte, respectively.

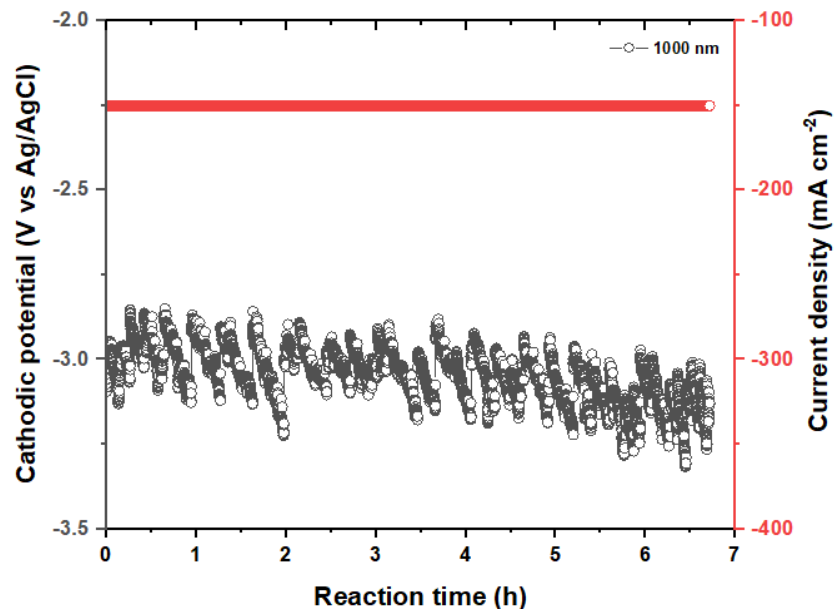


Fig. S7. Potential data of continuous electrochemical CO₂ reduction reactions at -150 mA cm⁻² on 1000nm Cu sample. 1M KHCO₃ and 1M KOH electrolytes were used as catholyte and anolyte, respectively.

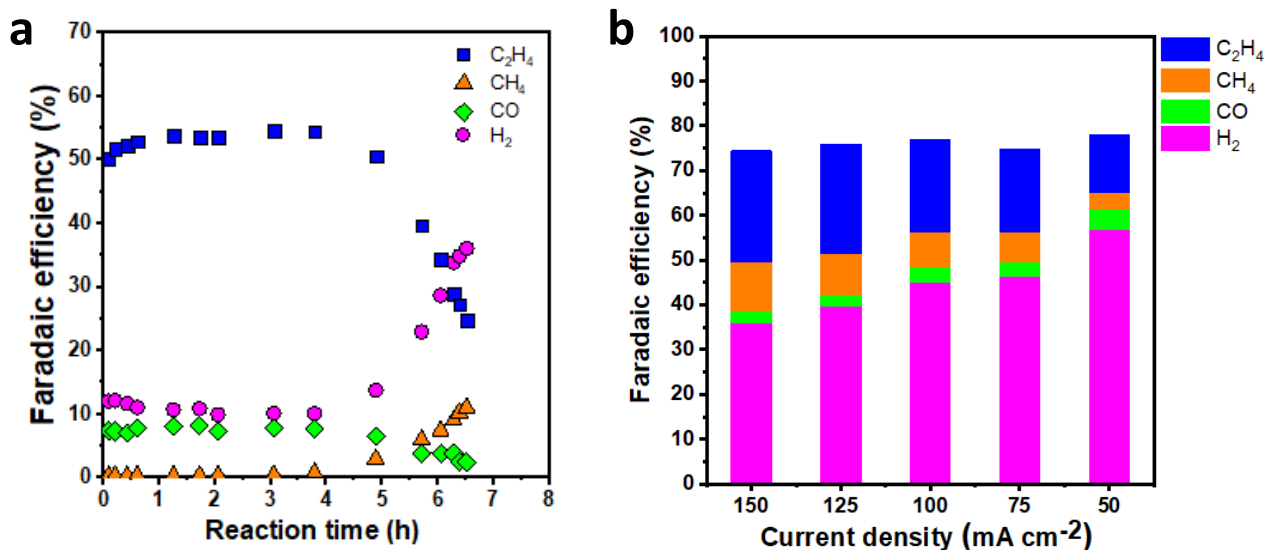


Fig. S8. Gaseous products distribution of the electrochemical CO₂ reduction of 1000 nm Cu/PTFE sample at low current densities. This experiment was carried out to confirm that the reason for the deactivation of the Cu catalyst after 5-6 h of continuous operation at -150 mA cm² was not the salt formation or flooding problem. The FE of C₂H₄ started at 50% and was maintained for 5 h before dropping sharply to about 25% within the next 1.5 h. The current density was then reduced to 125, 100, 75, and 50 mA cm⁻², and the gaseous products were analyzed accordingly. The FE's for H₂ and CH₄ remained high relative to their corresponding current densities, implying that CO₂ diffusion limitation was not the cause of the decrease in the FE of C₂H₄.

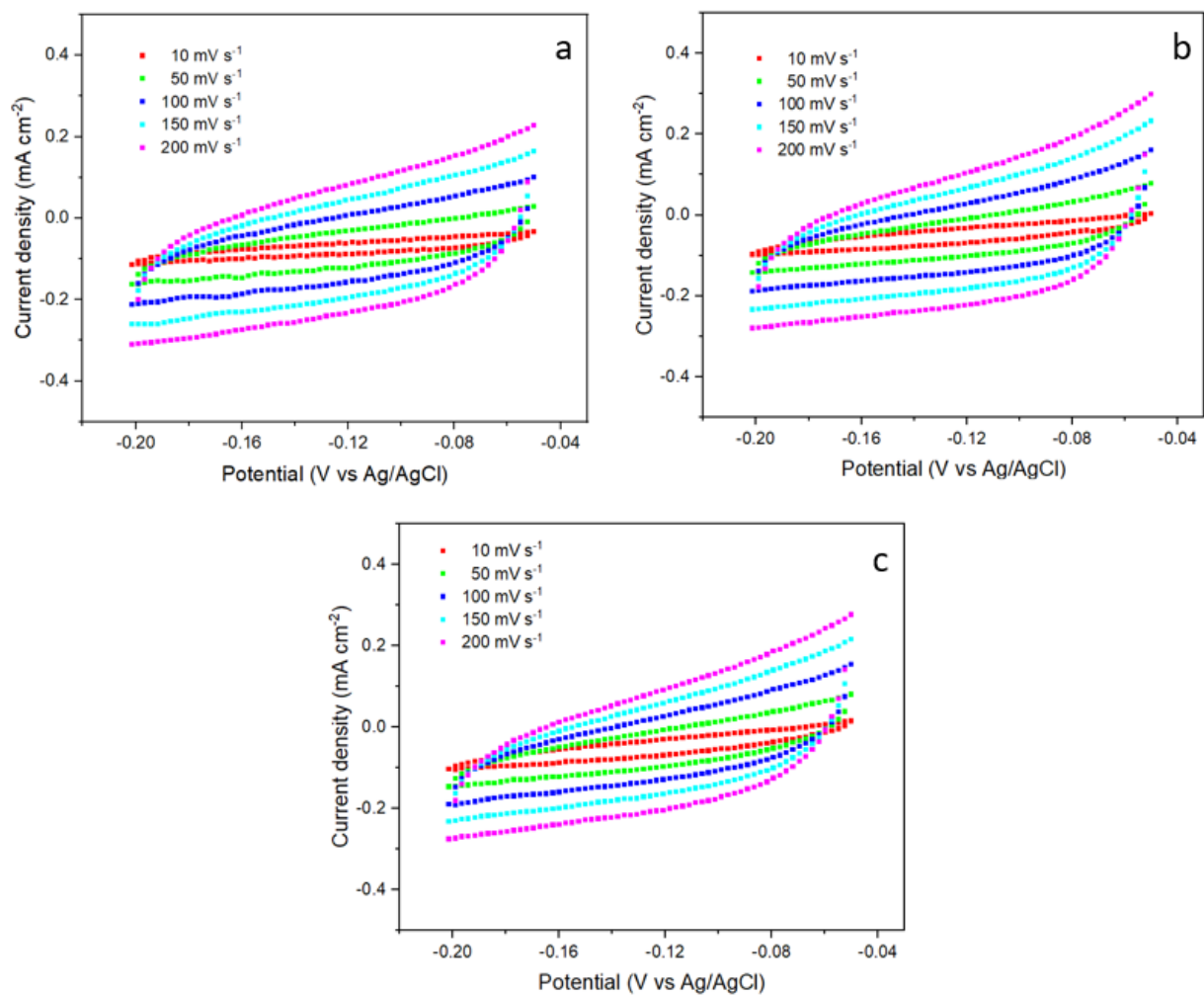


Fig. S9. Cyclic voltammety plot for (a) before electrolysis, (b) after 3 h of continuous electrolysis and (c) end of continuous electrolysis (6-7 h). The continuous electrolysis was carried out at a cathodic current density of 150 mA cm⁻².

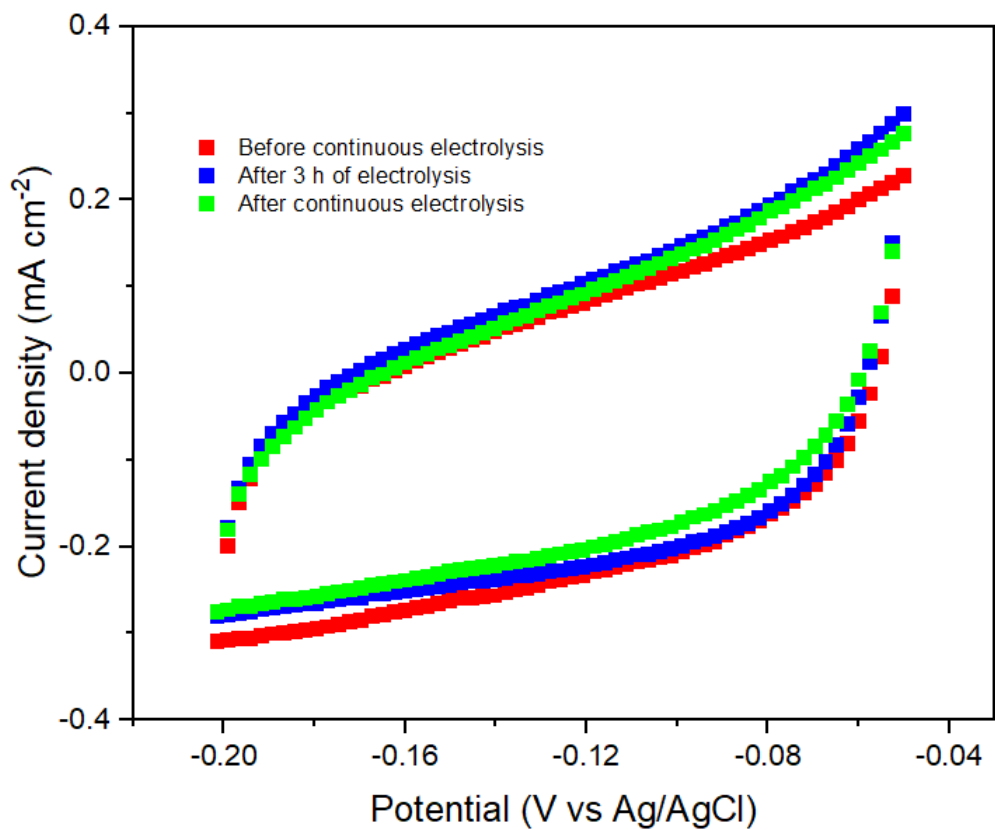


Fig. S10. Cyclic voltammetry scan using a scan rate of 200 mV s^{-1} showing the condition of the electrode-electrolyte interface before, during (after 3 h) and after (6-7 h) the continuous electrolysis. The continuous electrolysis was carried out at a cathodic current density of 150 mA cm^{-2} .

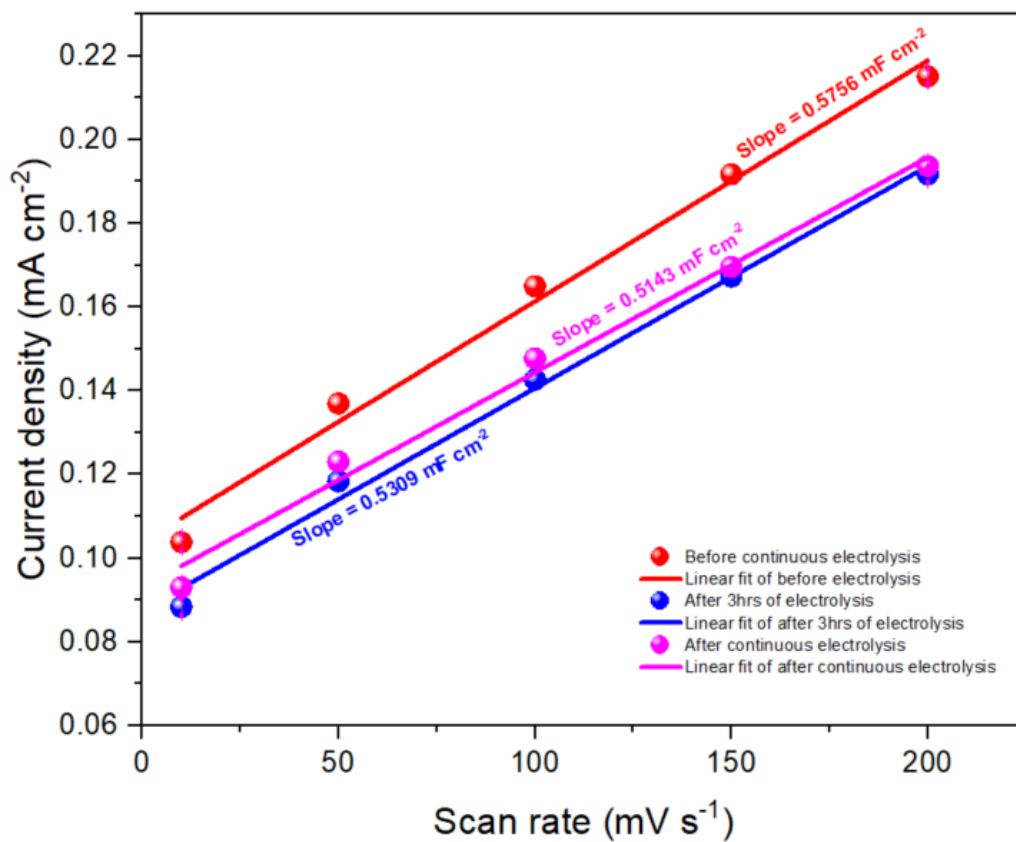


Fig. S11. Charging current density at -0.20 V (vs Ag/AgCl) versus scan rate and linear fit for the estimation of electric double layer capacitance.

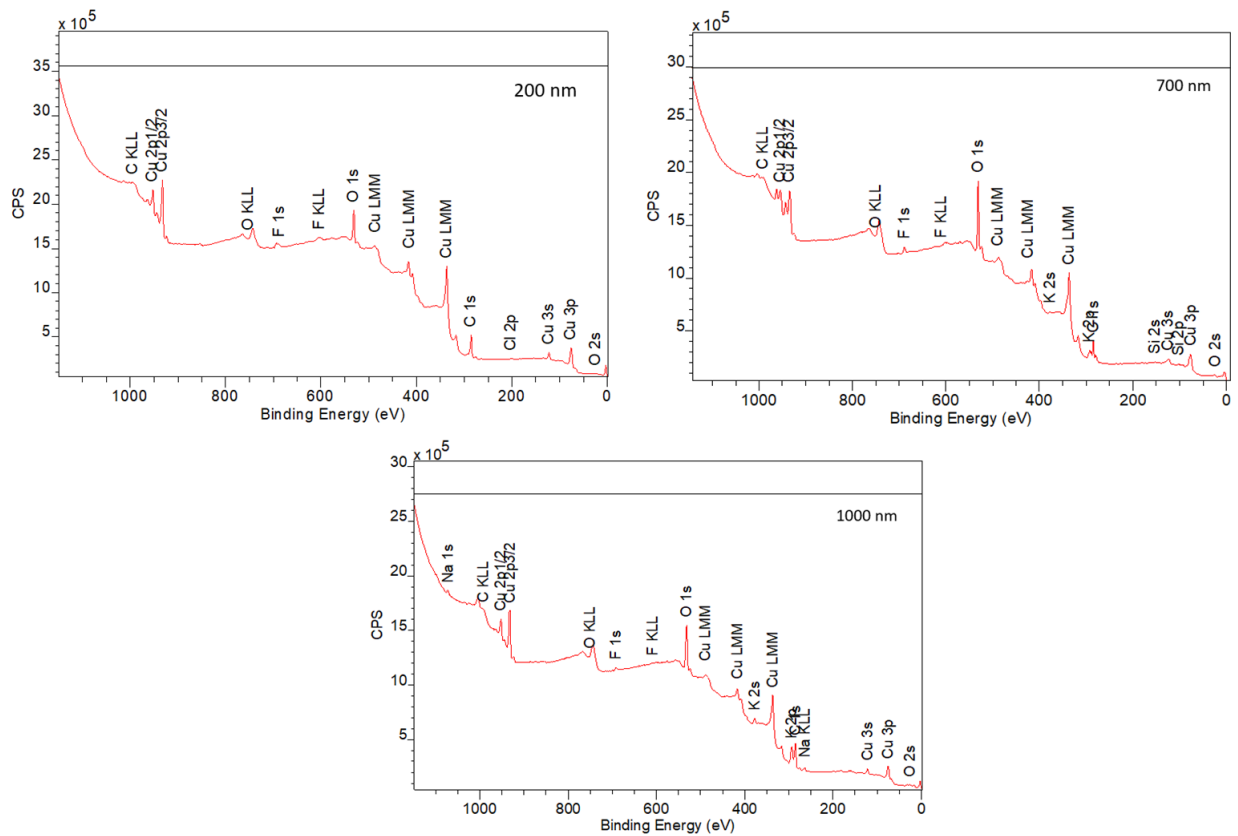


Fig. S12. X-ray photoelectron spectroscopy (XPS) of 200nm, 700nm and 1000nm spent Cu/PTFE samples after continuous electrolysis to confirm the presence of impurities.

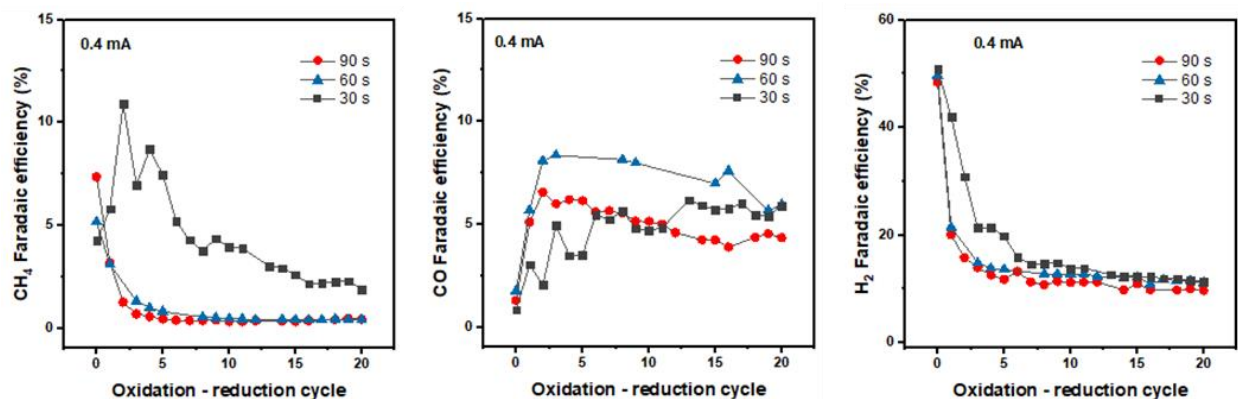


Fig. S13 Regeneration of Cu catalyst by *in-situ* oxidation. Gaseous product distribution for the recovery of FE for CH₄, CO, and H₂ at oxidation current density of 0.4 mA cm⁻² with different oxidation time. Products were collected at the end of each reduction cycle. For a given deactivated Cu catalyst and at the selected oxidation current density, the FE of H₂ at cycle “0” (FE of H₂ on the deactivated catalyst, just before the start of regeneration) was highly suppressed from almost 50% to about 15-17% within the first 5 cycles. Also, the FE of CH₄ and CO were similarly recovered showing that the periodic refreshing of the active Cu catalytic site via oxidation can be used to prolong the catalyst operation lifetime. Oxidation time was also observed to have an impact at all oxidation current densities. Longer oxidation time shows quicker recovery. The same trends were also observed in Fig. S10 – S12, for 0.6, 0.8, and 1 mA cm⁻² oxidation current densities.

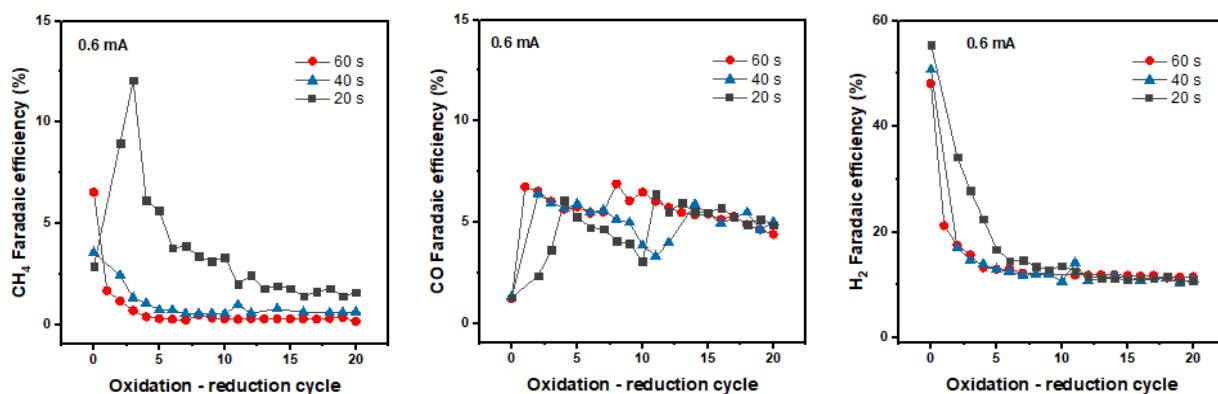


Fig. S14. Regeneration of Cu catalyst by *in-situ* oxidation. Gaseous product distribution for the recovery of FE for CH₄, CO and H₂ at oxidation current density of 0.6 mA cm⁻² with different oxidation time. Products were collected at the end of each reduction cycle.

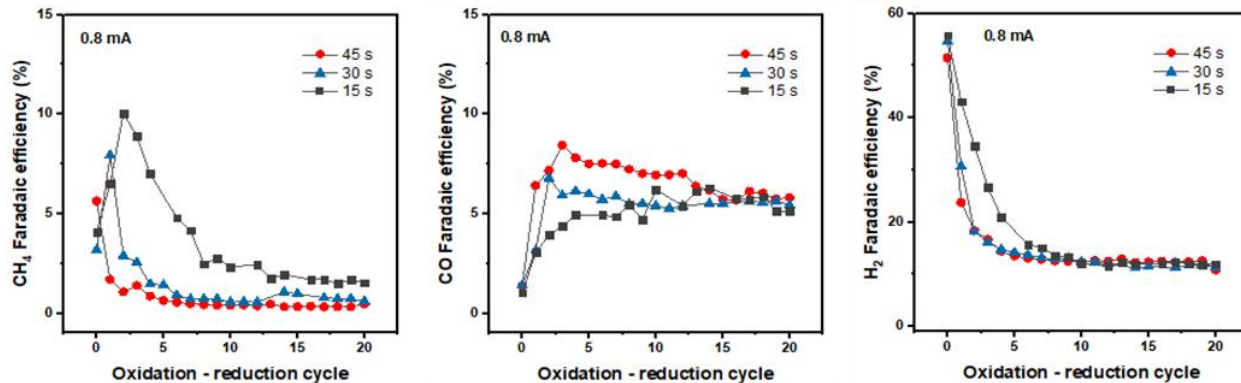


Fig. S15. Regeneration of Cu catalyst by *in-situ* oxidation. Gaseous product distribution for the recovery of FE for CH₄, CO and H₂ at oxidation current density of 0.8 mA cm⁻² with different oxidation time. Products were collected at the end of each reduction cycle.

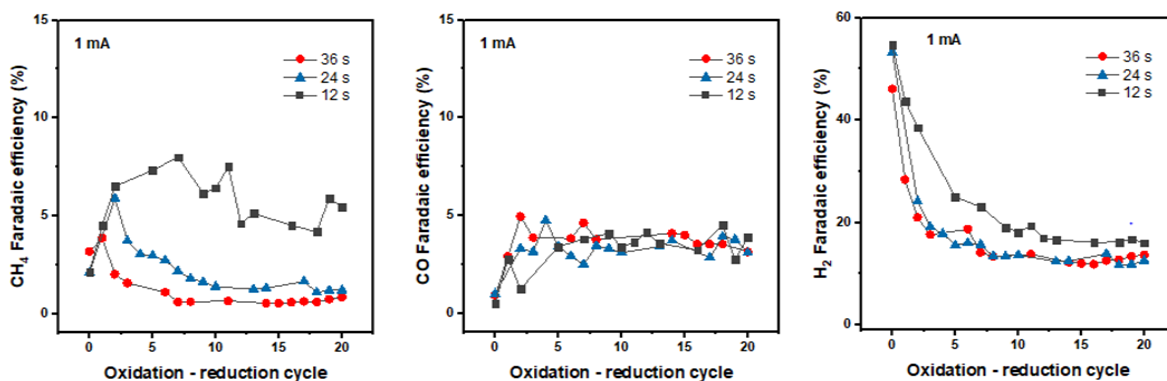


Fig. S16. Regeneration of Cu catalyst by *in-situ* oxidation. Gaseous product distribution for the recovery of FE for CH₄, CO and H₂ at oxidation current density of 1 mA cm⁻² with different oxidation time. Products were collected at the end of each reduction cycle.

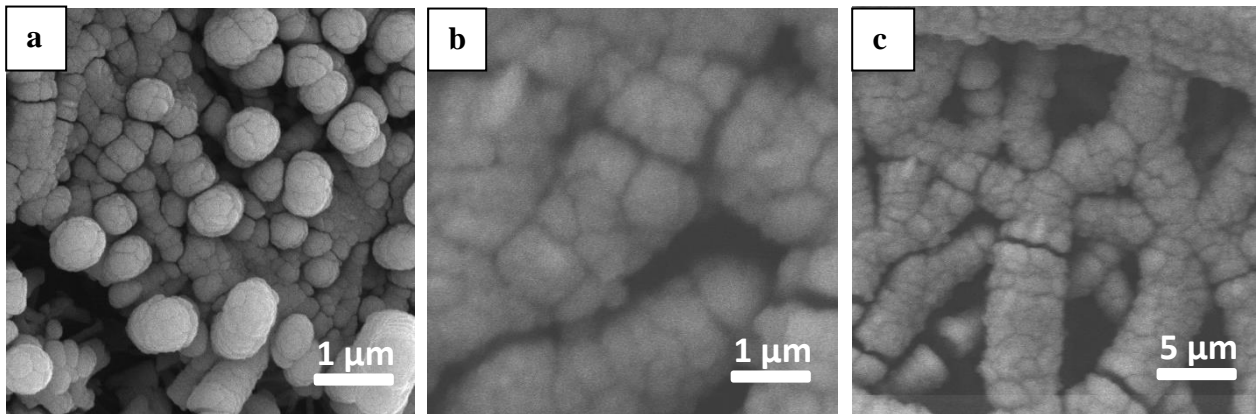


Fig. S17. (a) Cu/PTFE morphology before electrolysis. (b) and (c) Cu/PTFE morphology after in-situ electrooxidation test. The surface texture of Cu/PTFE appeared to change after series of electrooxidation reaction as the particle size seems broken into smaller sizes.

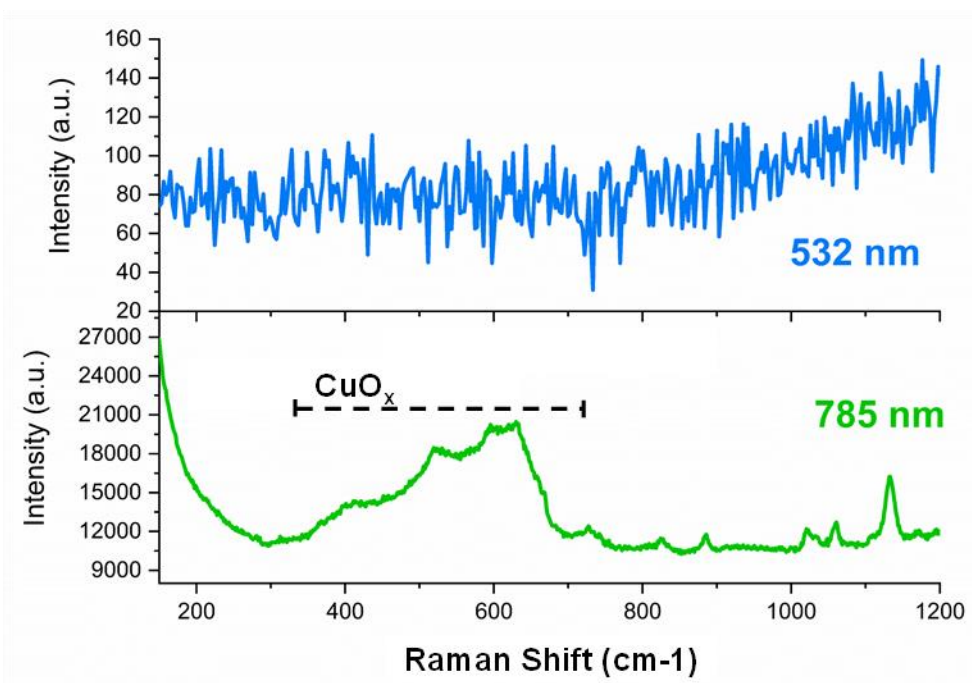


Fig. S18. In Situ Raman measurement signal enhancement. Raman spectra from the surface of sputtered copper with two different laser wavelengths (532 nm laser excitation and 785 nm laser excitation). A control experiment with two different laser wavelengths to study the effect of laser excitation wavelength.

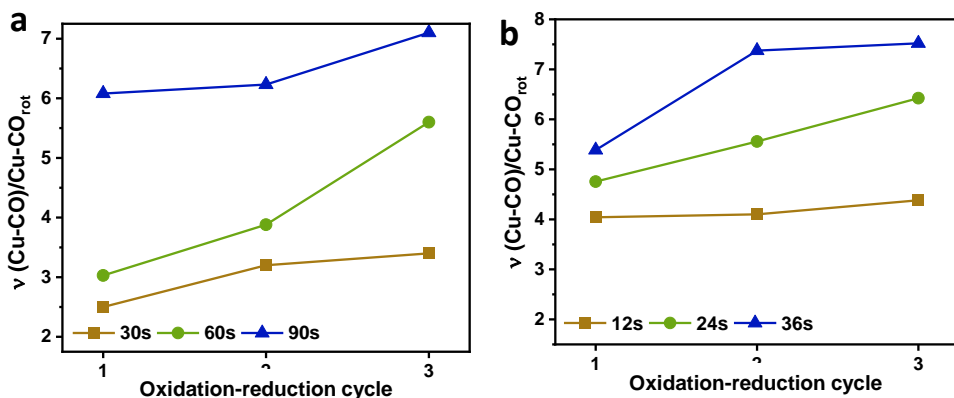


Fig. S19. In situ Raman analysis of Cu/PTFE catalysts. Peaks intensity ratios for (a) 0.4 mA cm^{-2} and (b) 1.0 mA cm^{-2} oxidation current density at different cycles and different oxidation time.

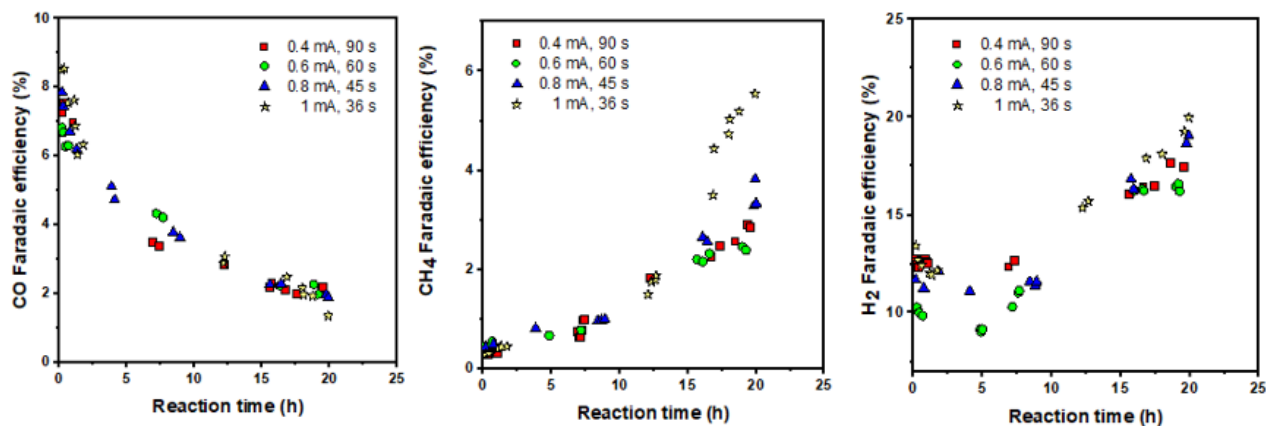


Fig. S20. Oxidation charge Optimization. Variation of CO, CH₄ and H₂ FE over the reaction lifetime at a constant current density of 150 mA cm^{-2} for 5 min reduction time in 1 M KHCO₃ electrolyte. When the regeneration strategy was applied to a fresh Cu catalyst, the FE of CO decreased significantly and in similar trends with increasing reaction time for all oxidation currents and time scenarios. This shows that varying combinations of oxidation current density and time plays a negligible role in as much as the oxidation charge was fixed. The FE's of CH₄ and H₂ were observed to increase over time as the reaction progressed, leading to a gradual decrease in the FE of C₂H₄.

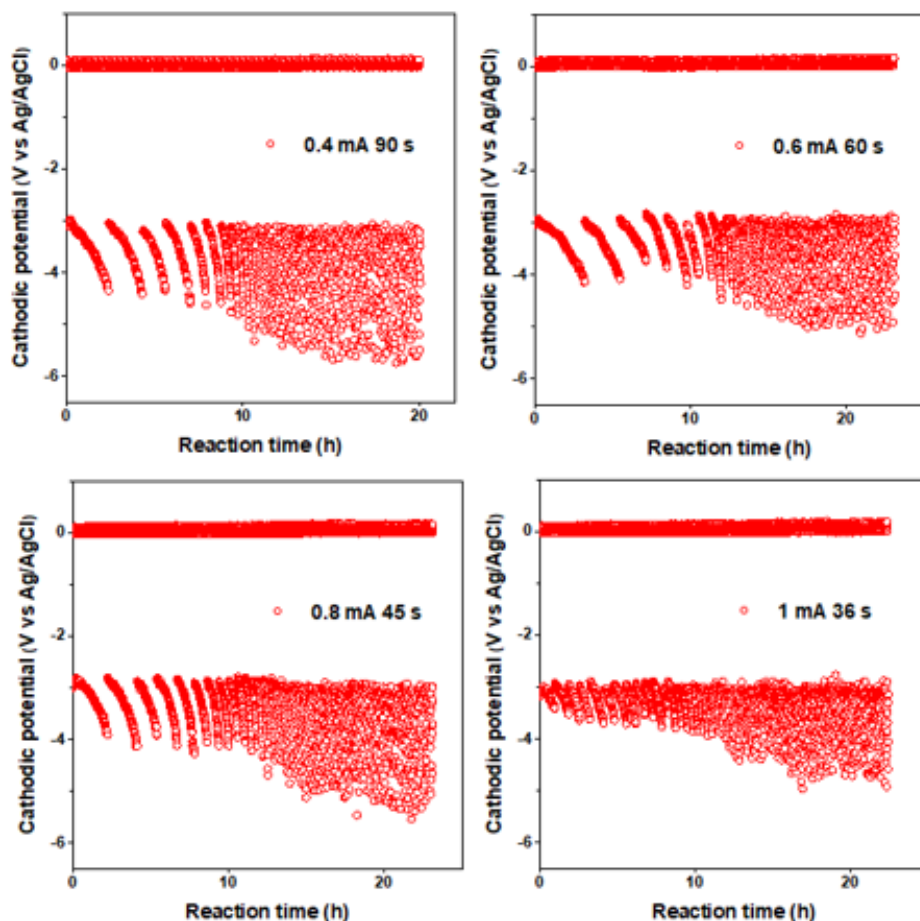


Fig. S21. Potential versus reaction time plot for oxidation charge optimization at a fixed current density of 150 mA cm^{-2} for 5 min reduction time and a fixed oxidation charge of 36 mC.

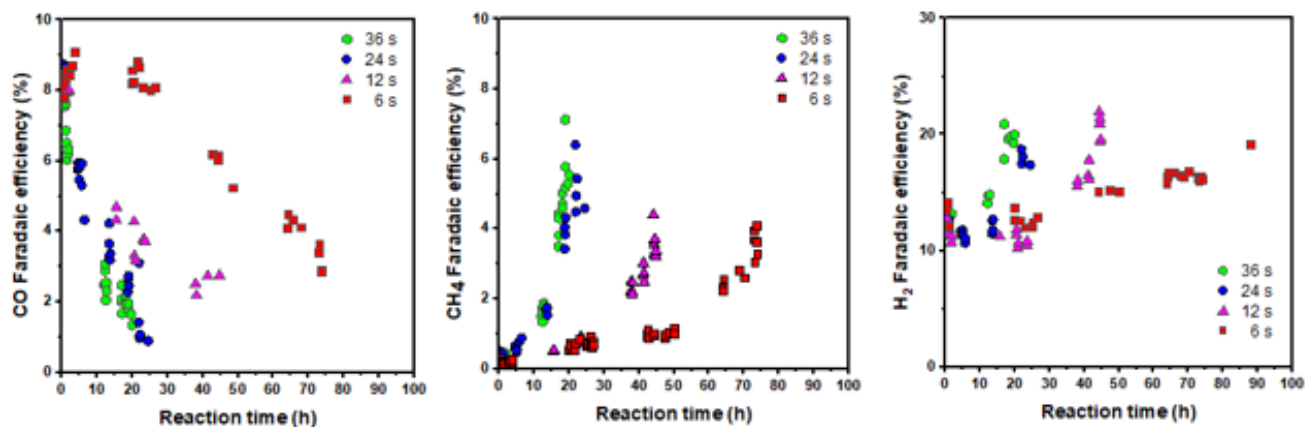


Fig. S22. Oxidation time optimization. Variation of CO, CH₄, and H₂ FE over the reaction lifetime for oxidation time optimization at a fixed current density of 150 mA cm^{-2} for 5 min reduction time and an oxidation current of 1 mA (the oxidation time was varied between 6s and 36 s). Lower oxidation time showed more stability, howbeit, with a lower C₂H₄ FE for the most part of the

stability testing period. For 6 s oxidation time, the drop in FE of CO was about 6%, while CH₄ and H₂ increase was about 4% and 8-9% respectively in almost 75 h operation time. In a 20 h of operation, the FE of CO dropped 6-7%, while CH₄ and H₂ increased by about 7% and 10% respectively in an oxidation time of 36 s. This shows that time, and consequently current matters when oxidation charge is varied. But both cannot be simultaneously controlled to obtain a relatively high FE for C₂H₄. This, therefore, suggests a different deactivation mechanism from the major ones outlined in the literature.

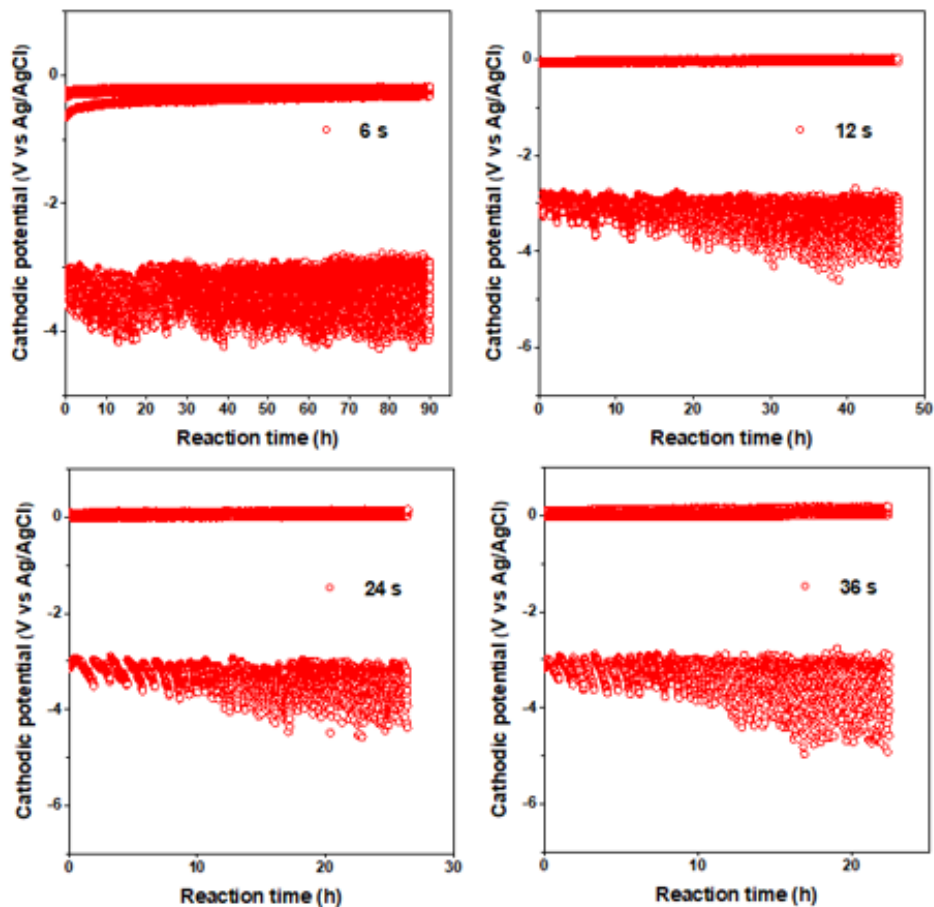


Fig. S23. Potential versus reaction time plot for oxidation time optimization at a fixed current density of 150 mA cm⁻² for 5 min reduction time and a fixed oxidation current density of 1 mA cm⁻² with oxidation time varied between 6 s and 36 s.

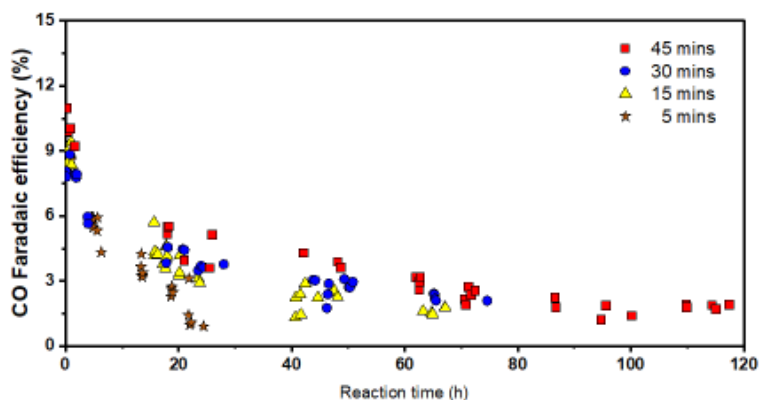


Fig. S24. Reduction time optimization. Variation of CO FE over the reaction lifetime for reduction time optimization at a fixed current density of 150 mA cm^{-2} , fixed oxidation current density, and time of 1 mA cm^{-2} and 24 s , respectively. With the optimization of the oxidation charge, values $\geq 24 \text{ mC}$ were observed to be the minimum required to reactivate a deactivated Cu catalyst, at least back to the range of its starting FE. Hence, using an oxidation current density of 1 mA cm^{-2} and 24 s oxidation time, the reduction time was optimized. The Cu catalyst was able to achieve an operation lifetime of about 120 h , compared to $5\text{-}6 \text{ h}$ of operation when allowed to run continuously. The FE of CO dropped by approximately 10% , while CH_4 and H_2 FE's increased by 4% and $2\text{-}5\%$ respectively

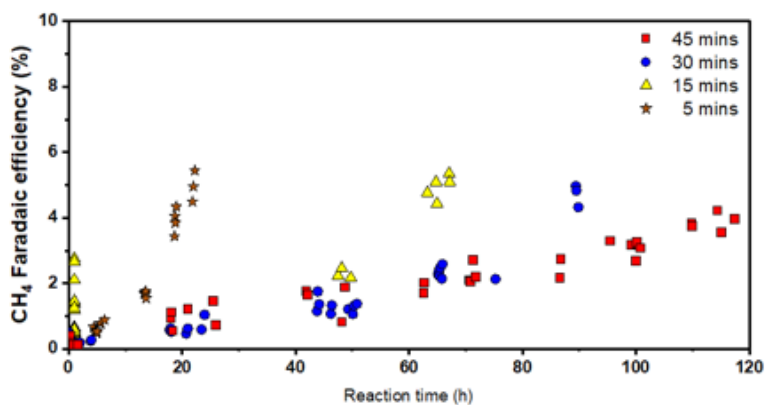


Fig. S25. Reduction time optimization. Variation of CH_4 FE over the reaction lifetime for reduction time optimization at a fixed current density of 150 mA cm^{-2} , fixed oxidation current density, and time of 1 mA and 24 s , respectively.

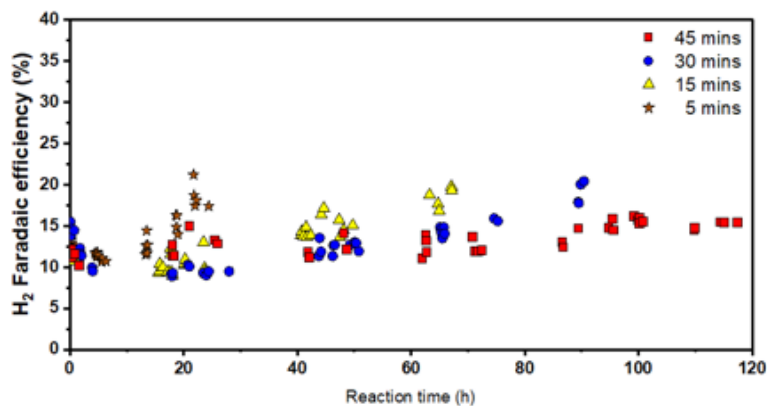


Fig. S26. Reduction time optimization. Variation of H₂ FE over the reaction lifetime for reduction time optimization at a fixed current density of 150 mA cm⁻² and fixed oxidation current density, and time of 1 mA and 24 s, respectively.

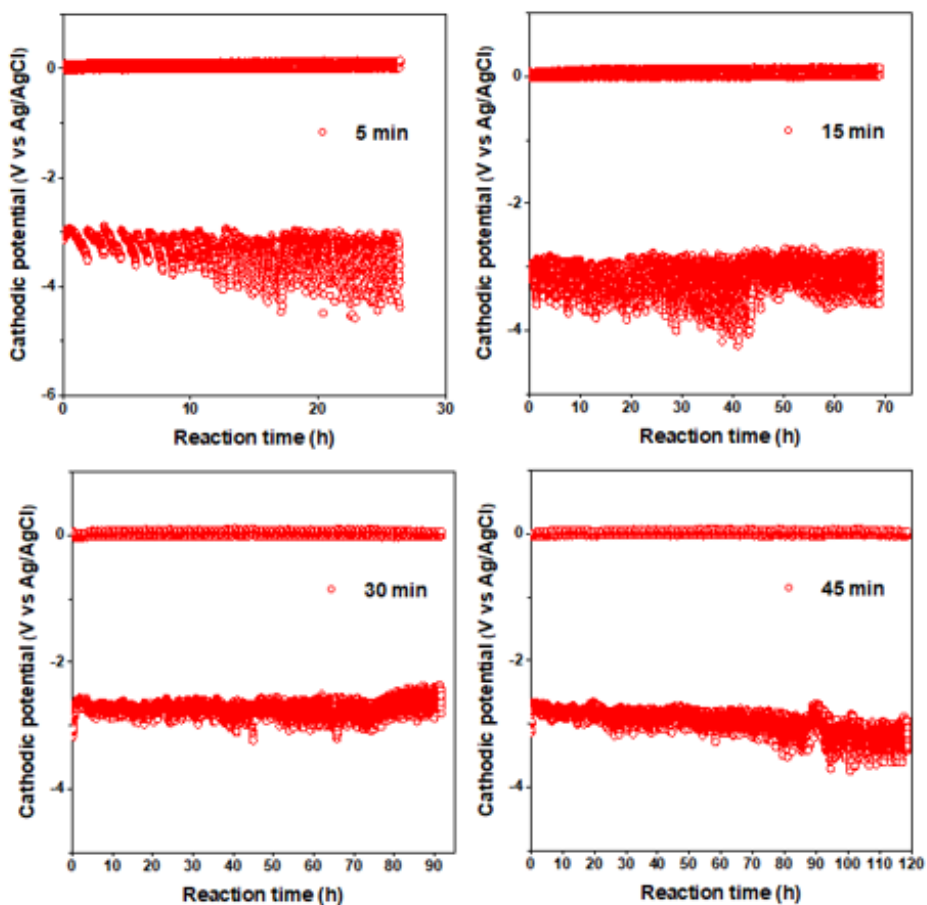


Fig. S27. Potential versus reaction time plot for stability of the Cu/PTFE catalysts with the optimized alternating current strategy in 1M KHCO₃. Reduction time optimization of 5 min, 15 min, 30 min and 45 min at a fixed oxidation current density and time of 1 mA cm⁻² and 24 s respectively.

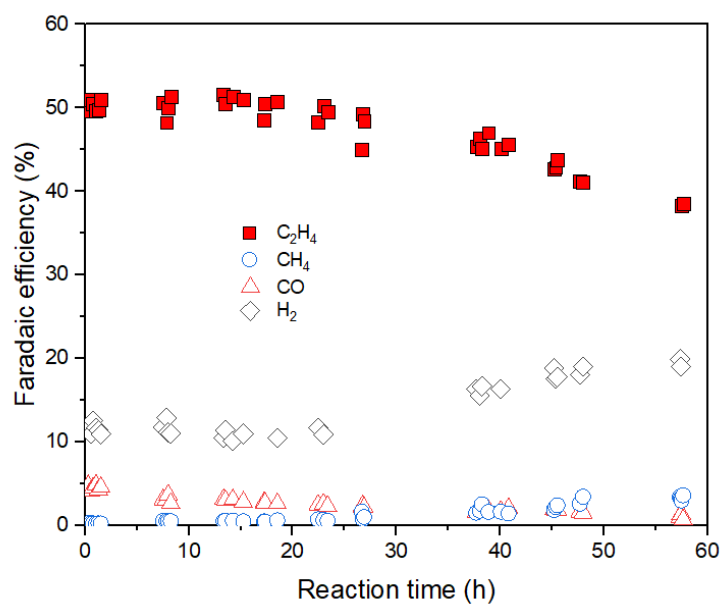


Fig. S28. Stability testing at higher oxidation charge 60 mC (1 mA, 60 s) and reduction at -150 mA cm⁻² for 45 mins.

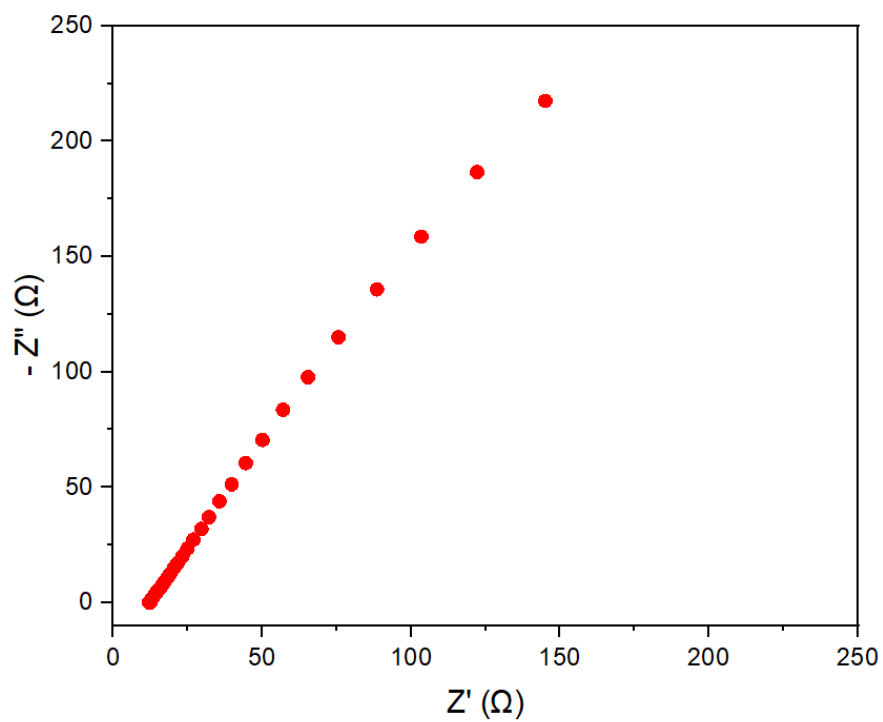


Fig. S29. Determination of cell resistance using electrochemical impedance spectroscopy measurement.

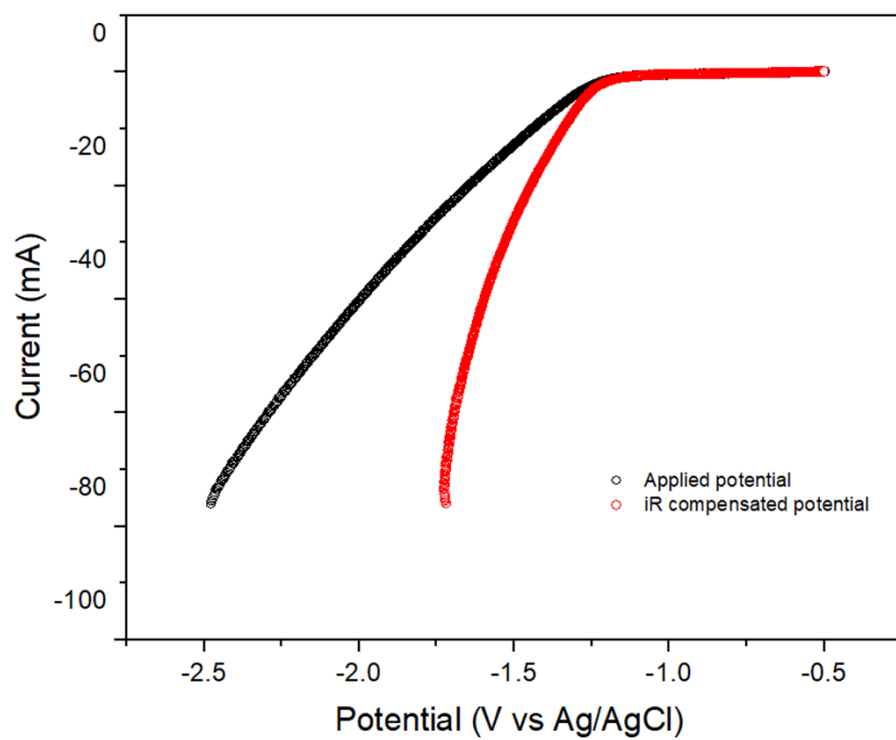


Fig. S30. iR correction determined from the electrochemical workstation and the compensated potential plot.